Macromolecular Materials and Engineering

Macromolecular Materials and Engineering Open Access
www.mame-journal.de

RESEARCH ARTICLE OPEN ACCESS

Film Blowing of Biobased Biodegradable Polyesters: Poly (Pentylene Adipate-co-Terephthalate) and Poly (Dodecylene Furanoate)

Hesham Aboukeila[1] | Onkar Singh[1] | Mahdi Mazaheri[1] | Emily Edwards[1] | Mason A. Rhue[1] | John Klier[1] | George W. Huber[2] | Brian P. Grady[1]

[1]School of Sustainable Chemical, Biological and Materials Engineering, University of Oklahoma, Norman, Oklahoma, USA | [2]Department of Chemical and Biological Engineering, University of Wisconsin-Madison, Madison, Wisconsin, United States

Correspondence: Brian P. Grady (bpgrady@ou.edu)

Received: 5 June 2025 | **Revised:** 17 August 2025 | **Accepted:** 4 September 2025

Funding: U.S. Department of Energy (DE-EE0009305), and National Science Foundation (CMMI-2216074).

Keywords: biodegradable | compression molded | film blowing | furandicarboxylic acid | pentanediol | polyesters

ABSTRACT

Poly(pentylene adipate-co-terephthalate) (PPeAT), poly (dodecylene furanoate) (PDDF), polybutylene adipate terephthalate (PBAT), and linear low-density polyethylene (LLDPE) films were prepared using film blowing. Machine direction (MD) and transverse direction (TD) properties of the blown films (BFs) are compared to the properties of compression molded sheets (CMSs). For all polymers, Young's modulus, stress at break elongation at break and storage modulus are higher for the CMSs vs. BFs. PPeAT films have a higher modulus than PBAT films demonstrating its superior mechanical properties. X-ray scattering shows that CMSs have higher percent crystallinity, longer d-spacing, and larger crystal size compared with BFs. For BFs, SAXS measurements have more intensity in the MD vs. the TD while the d-spacing is slightly higher for the MD; however, WAXS results indicate that films in the TD have higher percent crystallinity than in the MD. CMSs exhibit lower oxygen permeability, carbon dioxide permeability, and normalized water vapor transmission rates compared with BFs consistent with the higher crystallinity. Biobased, biodegradable PPeAT and PDDF show lower oxygen and carbon dioxide permeabilities compared with fossil fuel-based PBAT and LLDPE and lower water vapor transmission rates than PBAT. PPeAT and PDDF BFs show promising results and eventually might be used as a drop-in replacement for LLDPE in flexible film packaging.

1 | Introduction

Linear low-density polyethylene (LLDPE) and low-density polyethylene (LDPE) are two of the most used polymers for flexible film packaging [1, 2]. LLDPE is known for its excellent tensile strength and puncture resistance, making it highly suitable for applications that require durability and flexibility. Incorporating small quantities of LDPE into LLDPE significantly enhances extensional viscosity and introduces some strain-hardening properties [3]. Both LLDPE and LDPE offer significant advantages such as low cost, high availability, and versatility, which have driven their widespread use in packaging, agriculture, and other industries [4]. However, these advantages come with notable drawbacks. LLDPE and LDPE are derived from non-renewable petroleum resources and are not biodegradable, contributing significantly to plastic waste pollution [5, 6]. The persistence of these plastics in the environment poses a serious threat to wildlife and ecosystems, as well as contributing to the growing problem of microplastics [7–9]. The durability that makes these materials so useful also makes

them problematic in terms of disposal and environmental impact. Hence, there is an urgent need for biodegradable alternatives that can provide similar thermal, mechanical, and barrier properties without the associated environmental problems [10].

The increasing global focus on the fate of plastics in the environment has driven the development of biodegradable polymers [11]. Among these, polybutylene adipate terephthalate (PBAT), has emerged as a promising biodegradable polyester. PBAT is a biodegradable, aliphatic-aromatic copolyester that combines flexibility and durability. PBAT is synthesized from the polymerization of butanediol with a mixture of adipic acid and terephthalic acid, resulting in a material that possesses excellent thermal and barrier properties [12, 13]. PBAT is widely used in agricultural mulch films, and other disposable products due to its ability to break down under composting conditions [14]. PBAT's compatibility with other biopolymers, like polylactic acid (PLA) and starch, further enhances its versatility, enabling the development of composite materials with improved performance characteristics tailored for specific applications [15, 16]. PBAT is produced commercially by leading companies such as BASF [17], Novamont [18], LG Chem [19] and SK Global [20]. However, due to its low Young's modulus, PBAT is almost always used in a blend for flexible film packaging [21].

Poly(pentylene adipate-co-terephthalate) (PPeAT) with a 40/60 adipic acid/terephthalic acid mole percent exhibits mechanical properties that are comparable to linear low-density polyethylene (LLDPE), a widely used conventional plastic [21, 22]. Pentanediol is typically biosourced, while butanediol is not. PPeAT and PBAT are compostable; LLDPE is certainly not and even PLA is not. Additionally, PPeAT stands out for its superior mechanical performance when compared to PBAT, having ~double the Young's modulus of PBAT. This enhanced performance of PPeAT, particularly in terms of Young's modulus, positions it as a robust alternative to traditional petroleum-based plastics and other biodegradable plastics. Our prior studies involved a thorough characterization of the polymer's properties, confirming its suitability for film blowing due to its favorable rheological and mechanical behavior [21]. The main drawback of neat PPeAT is the very slow crystallization kinetics which was overcome by adding a nucleating agent [21]. Without the nucleating agent, PPeAT could not have been blown into a film because the solidification time would have been too long.

Additionally, poly (dodecylene furanoate) (PDDF) has shown potential for food packaging applications due to the similar Young's modulus and significantly better gas barrier properties compared to conventional materials such as LDPE and LLDPE [23]. Although PDDF is not considered a biodegradable polymer according to ASTM standards, PDDF biodegrades significantly faster than LDPE and LLDPE, breaking down within 990 days in freshwater environments and 475 days in composting conditions. Furthermore, as with PBAT and PPeAT, PDDF can be easily chemically recycled to obtain the original monomers using hydrolysis or methanolysis [23].

Film blowing is favored over compression molding for the production of films for many reasons, including its ability to create thin, uniform, and continuous films with high production rates [24]. In film blowing, the polymer is melted and extruded through a circular die to form a thin tube, which is then inflated to produce a film. This process allows for precise control over film thickness, crystal size, and chain orientation by adjusting parameters such as extrusion speed, blow-up ratio, blow-up air temperature, drawdown ratio, velocity of nip rolls, and type of bubble inflation [25, 26]. Film blowing is particularly advantageous for producing large quantities of film with consistent quality, making it ideal for applications like packaging [27] and agricultural [28] applications. Polymers that can be processed by film blowing include LLDPE [29], LDPE [30, 31], ethylene vinyl alcohol [32], polystyrene [33], polyethylene terephthalate [34], PBAT [35], PLA [36], and polyhydroxyalkanoate [37]. In contrast, compression molding involves placing a polymer in a heated mold, applying pressure, and then cooling it to form a solid part. While compression molding is effective for creating thicker and more complex shapes [38], compression molding is much less efficient and much more limited in producing the continuous, thin films required for flexible packaging.

In this work, blown films (BFs) of PPeAT, PDDF, PBAT and LLDPE were compared with compression molded sheets (CMSs) of the same polymers. BFs and CMSs were characterized using 2-D wide and small angle x-ray scattering (WAXS and SAXS) and dynamic mechanical analysis (DMA). Tensile and barrier properties were also measured. DMA and tensile tests were performed with samples cut in both the machine direction (MD) and transverse direction (TD) of the films. To the best of our knowledge, film blowing of PPeAT and PDDF, along with a comparative analysis against compression molded sheets, has not been previously explored.

2 | Results and Discussion

2.1 | Mechanical Properties

Stress-strain curves for CMSs as well as machine direction (MD) and transverse direction (TD) measurements of LLDPE, PBAT, PPeAT, and PDDF films are shown in Figure 1. Data presented here for PBAT compression molded sheet (CMS) were previously presented elsewhere [21]. However, data for PPeAT CMS (batches of material with different MW and without nucleator) and LLDPE CMS (different material with different MFI) have not been previously reported; however, both sets of results are close to those presented previously [21]. Young's modulus (E), stress at break (δ_b) and elongation at break (ε_b) were calculated and reported in Table 1. All four polymers exhibited ductile behavior with a high elongation at break. E, δ_b and ε_b values for the CMSs were higher than the BFs for all four polymers. The relative drop in E was approximately the same for LLDPE, PBAT and PPeAT at around 25%, while that for PDDF was almost 50%. Ultimate property drops (δ_b and ε_b) for LLDPE were only about 20%, while that for the polyesters was closer to 40%. The larger drop for the polyesters could be due to hydrolysis during processing; although the samples were dried prior to processing some degradation could have occurred. PPeAT BF exhibited a Young's modulus three times higher than that of PBAT BF and was comparable to LLDPE BF. Meanwhile, PDDF BF had a Young's modulus four times greater than PBAT BF and was similar to LLDPE BF.

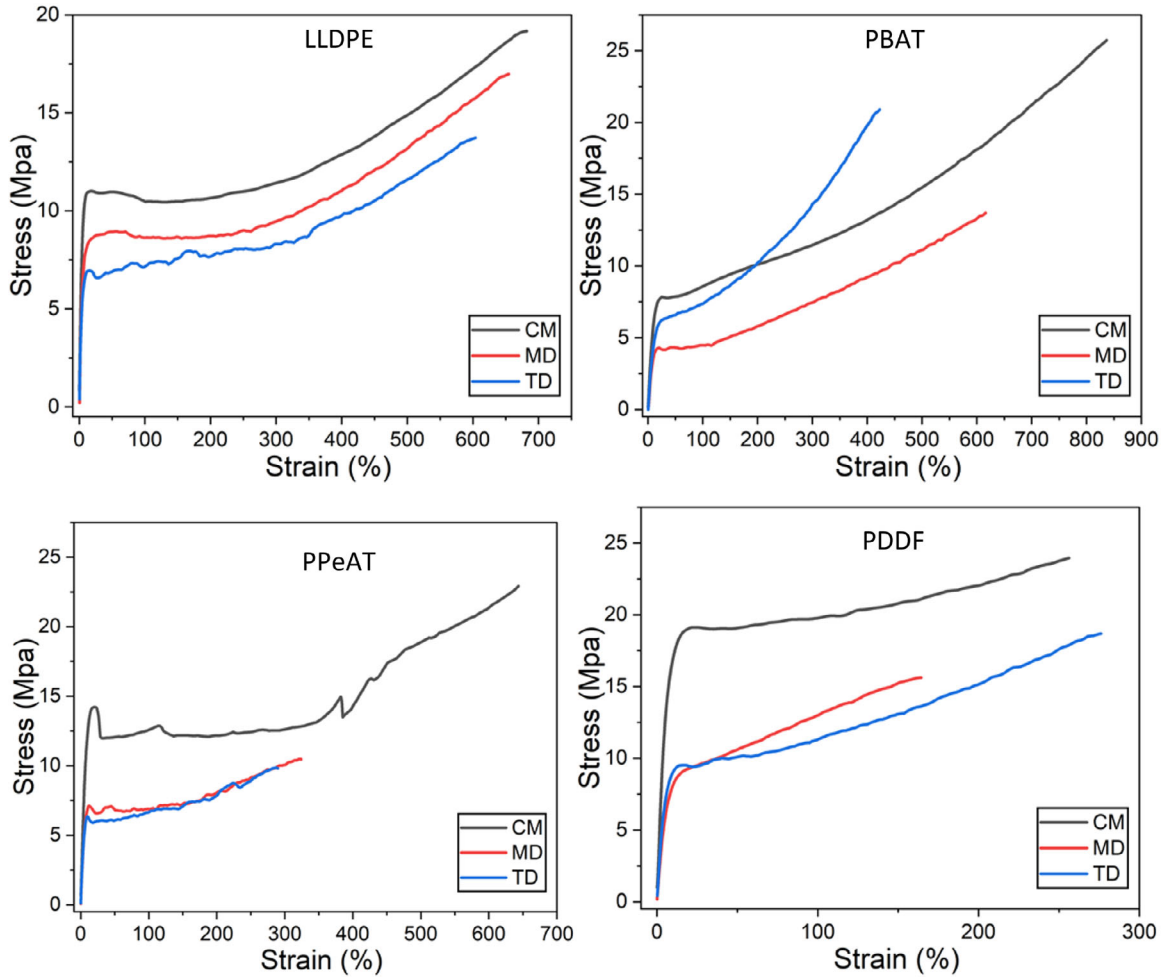

FIGURE 1 | Stress-strain curve of LLDPE, PBAT, PPeAT, and PDDF CMSs and BFs.

TABLE 1 | Mechanical properties of LLDPE, PBAT, PPeAT, and PDDF CMSs and BFs.

Samples		E MPa	δ_b MPa	ε_b %
LLDPE	**CMS**	230.0 ± 10.8	20.1 ± 3.8	707 ± 135
	MD	165.5 ± 35.5	16.7 ± 0.8	673 ± 27
	TD	165.8 ± 31.1	13.5 ± 2.1	580 ± 79
PBAT	**CMS**	78.0 ± 10.0	26.0 ± 3.0	815 ± 67
	MD	43.2 ± 6.8	13.9 ± 0.7	622 ± 25
	TD	50.2 ± 6.8	18.9 ± 3.0	414 ± 41
PPeAT	**CMS**	180.0 ± 5.8	22.5 ± 1.6	642 ± 49
	MD	131.7 ± 14.4	12.2 ± 1.5	334 ± 17
	TD	124.3 ± 29.3	9.5 ± 1.1	266 ± 38
PDDF	**CMS**	311.2 ± 6.0	24.0 ± 1.2	252 ± 24
	MD	163.4 ± 33.0	15.1 ± 2.5	147 ± 17
	TD	154.4 ± 24.0	18.7 ± 2.1	270 ± 47

For BFs, differences in Young's modulus between MD and TD were not statistically significant according to the Student's t-test at the 95% confidence interval for a given polymer. However, differences in stress at break and elongation at break between MD and TD was statistically significant for all polymers according to the Student's *t*-test. The elongation at break in the MD was higher than in the TD for LLDPE, PBAT, and PPeAT. At higher blow-up ratios, it has been previously demonstrated that the elongation at break in the TD exceeds that in the MD [39]. But for PDDF, the opposite held true, the elongation at break in the MD was higher than the elongation at break in the TD.

2.2 | Wide Angle X-Ray Scattering (WAXS)

Figure 2 shows WAXS spectra of the CMSs as well as BFs in the MD and TD for LLDPE, PBAT, PPeAT, and PDDF, while Table 2 reports the percent crystallinity values for these polymers. For PBAT, scattering angles ($2\theta^{\circ}$) observed are 16.2°, 17.3°, 20.4°, 23.2° and 24.8 corresponding to the planes (011), (010), (102), (100), and (111) respectively. For PPeAT, $2\theta^{\circ}$ are 15.9°, 17.4°, 21.8°, 23.5° and 25.5° with all peaks presumably corresponding to the same planes as for PBAT. However, a distinct peak at 7.6° was observed for PPeAT, which was not present in PBAT. For LLDPE, two sharp crystalline peaks can be observed at the $2\theta^{\circ}$ value 21.4° and 23.6° which are assigned to (110) and (200) planes. For PDDF, $2\theta^{\circ}$ are 9.8°, 17.9°, 21.6°, and 23.8° with the latter two scattering angles at approximately at the same angles as the planes (110), and (200) of LLDPE. CMSs exhibited a higher percent crystallinity compared

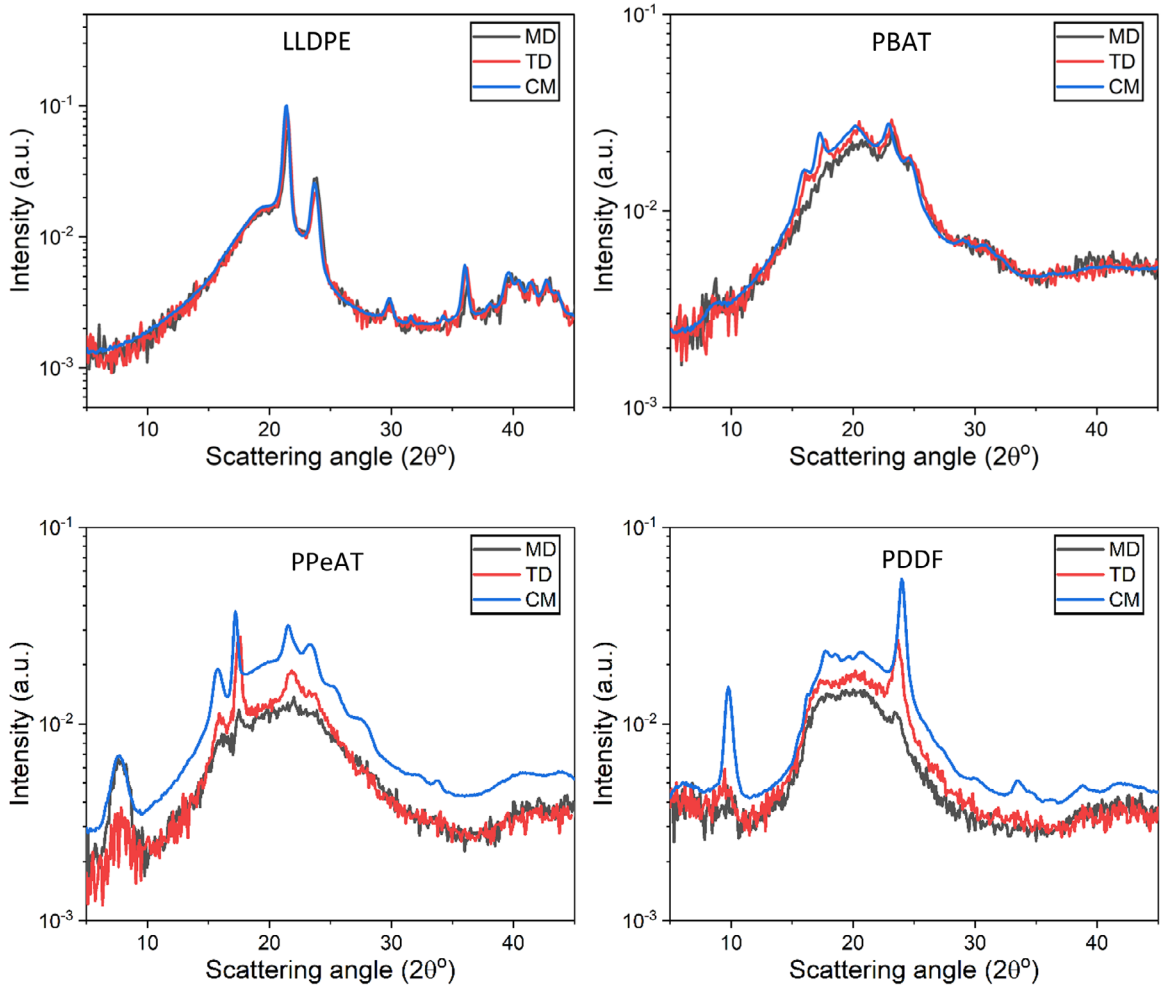

FIGURE 2 | Wide angle x-ray scattering results for LLDPE, PBAT, PPeAT, and PDDF CMSs and BFs.

TABLE 2 | Crystallinity properties of LLDPE, PBAT, PPeAT, and PDDF CMSs and BFs.

Samples		WAXS	SAXS				
		X_c %	q_{max} Å^{-1}	d-spacing Å	lamellar thick-ness Å	<cos2 ϕ> –	f –
LLDPE	**CMS**	41.8	0.034	184	76.8	0.33	0.00
	MD	36.8	0.040	156	57.3	0.35	0.03
	TD	38.2	0.038	165	63.1	n/a	n/a
PBAT	**CMS**	18.6	0.052	121	22.4	0.33	0.00
	MD	11.7	0.057	110	12.9	0.40	0.10
	TD	14.3	0.058	109	15.6	n/a	n/a
PPeAT	**CMS**	16.0	0.063	100	15.9	0.33	0.00
	MD	5.9	0.076	83	4.8	0.45	0.18
	TD	14.7	0.080	79	11.6	n/a	n/a
PDDF	**CMS**	36.1	0.049	128	46.1	0.33	0.00
	MD	14.8	0.058	109	16.2	0.41	0.12
	TD	25.8	0.068	920	23.8	n/a	n/a

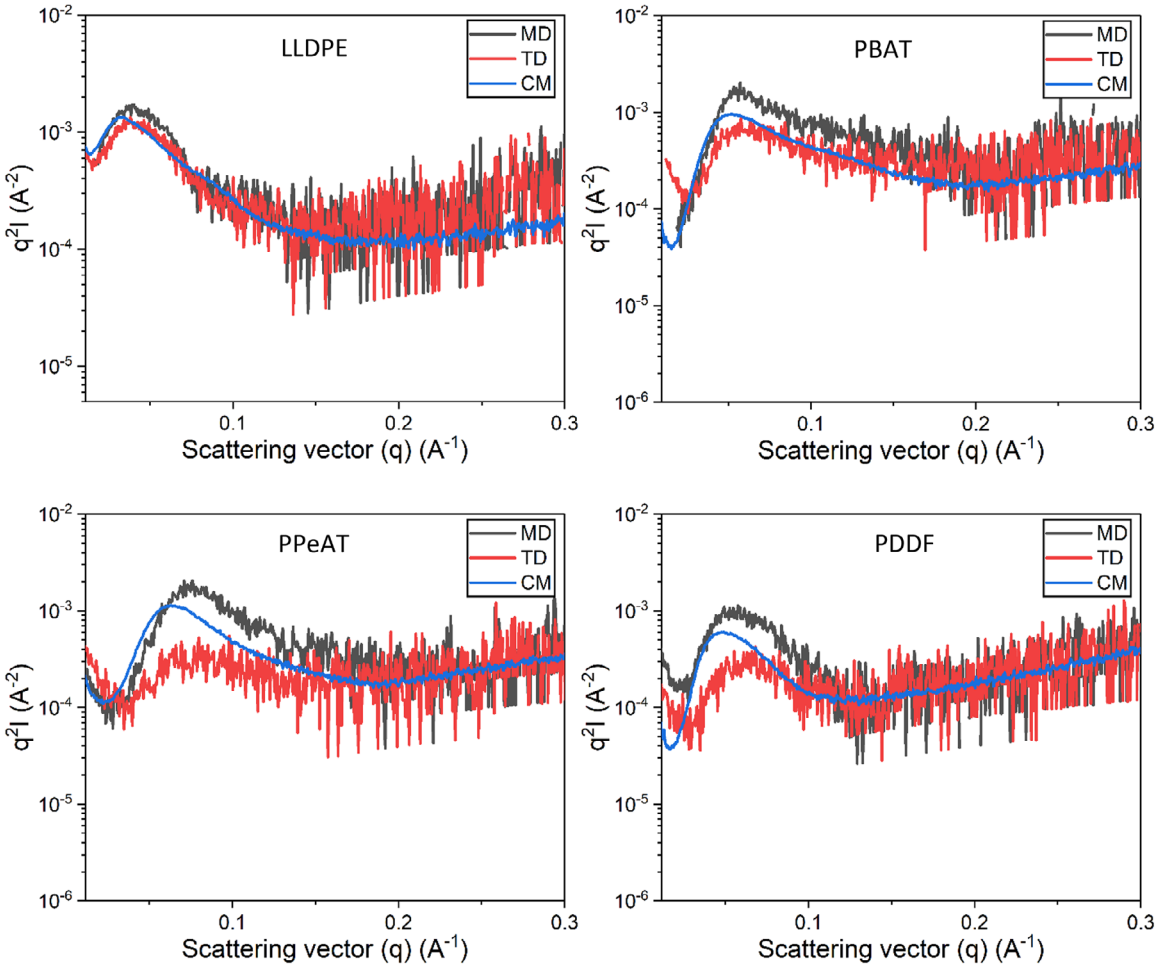

FIGURE 3 | Small angle x-ray scattering results for LLDPE, PBAT, PPeAT, and PDDF CMSs (Circularly averaged) and BFs (Sectionally averaged).

to both MD and TD BFs. This increase in crystallinity can be attributed to the gradual cooling process in compression molding, which allows polymer molecular chains to organize into a more ordered structure [40, 41]. The higher degree of crystallinity of CMSs compared to BFs almost certainly contributed to the higher Young's modulus for CMSs shown in Table 1. Blown films (BFs) in the TD had a higher percent crystallinity than in the MD. PBAT, PPeAT and PDDF had a high cooling rate (air blower: 2000 RPM) vs. a lower cooling rate for LLDPE (air blower: 1020 RPM), which could explain why the WAXS patterns for the MD and TD were more similar for the latter. Higher cooling rate for polyesters alongside a lower screw speed and haul-off speed were used so that the film thicknesses would approximately match; fundamentally, the difference required in cooling rate to match final film thickness is likely due to the slower crystallization rate of the polyesters compared to LLDPE. The reflections at ~16° and ~17° in both PBAT and PPeAT, and the reflection at ~7° in PPeAT showed a clear difference in intensity between MD and TD in favor of MD while the reflections at ~22°, ~23°, and ~25° showed a clear difference between MD and TD in favor of TD. For PDDF, the reflection at ~10° and ~24° showed a clear difference in intensity between MD and TD. Because the angles between these peaks and the chain direction/normal to the lamellae planes are not known, relating these results to the crystallite orientation is not possible. PPeAT films had a lower percent crystallinity compared to PBAT films, consistent with results obtained from the CMSs presented here as well as results on CMSs presented previously using a different batch of PPeAT [21]. PDDF BFs had a higher percent crystallinity compared to PBAT and PPeAT BFs, consistent with results obtained from CMSs.

2.3 | Small Angle X-Ray Scattering (SAXS)

Figure 3 and Table 2 show SAXS results for CMSs as well as BFs in the MD and TD for LLDPE, PBAT, PPeAT and PDDF. As these crystallites are anticipated to have a lamellar shape, peaks observed in $q^2I(q)$ vs. q represent characteristic long spacings derived from Bragg's law. The long period (d-spacing) was calculated using (Equation 1), where q_{max} is the value where $q^2I(q)$ vs. q was at peak maximum.

$$d = \frac{2\pi}{q_{max}} \quad (1)$$

Lamellar thicknesses reported in Table 2 are obtained by multiplication of fractional crystallinity with d-spacing values and represent a lower limit of the lamellar thickness since the density of the amorphous phase is less than the density of the crystalline phase. As expected, BFs have smaller d-spacings and thinner lamellar thicknesses than CMSs due to the faster cooling rate for film blowing. As previously mentioned, BFs in the TD have a higher percent crystallinity than in the MD, and these

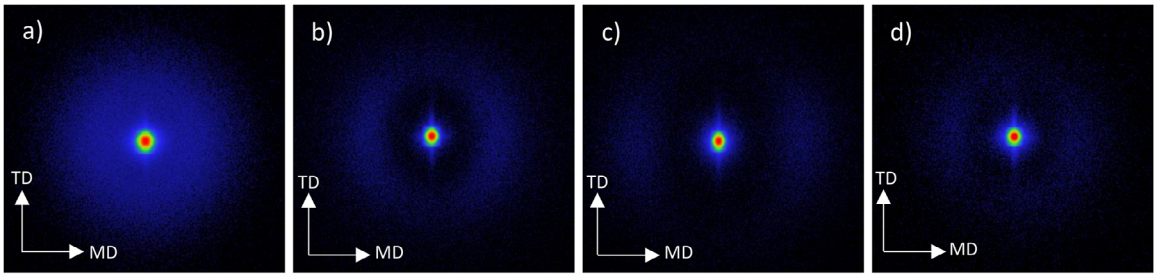

FIGURE 4 | Small x-ray scattering 2D images for a) LLDPE, b) PBAT, and c) PPeAT and d) PDDF BFs.

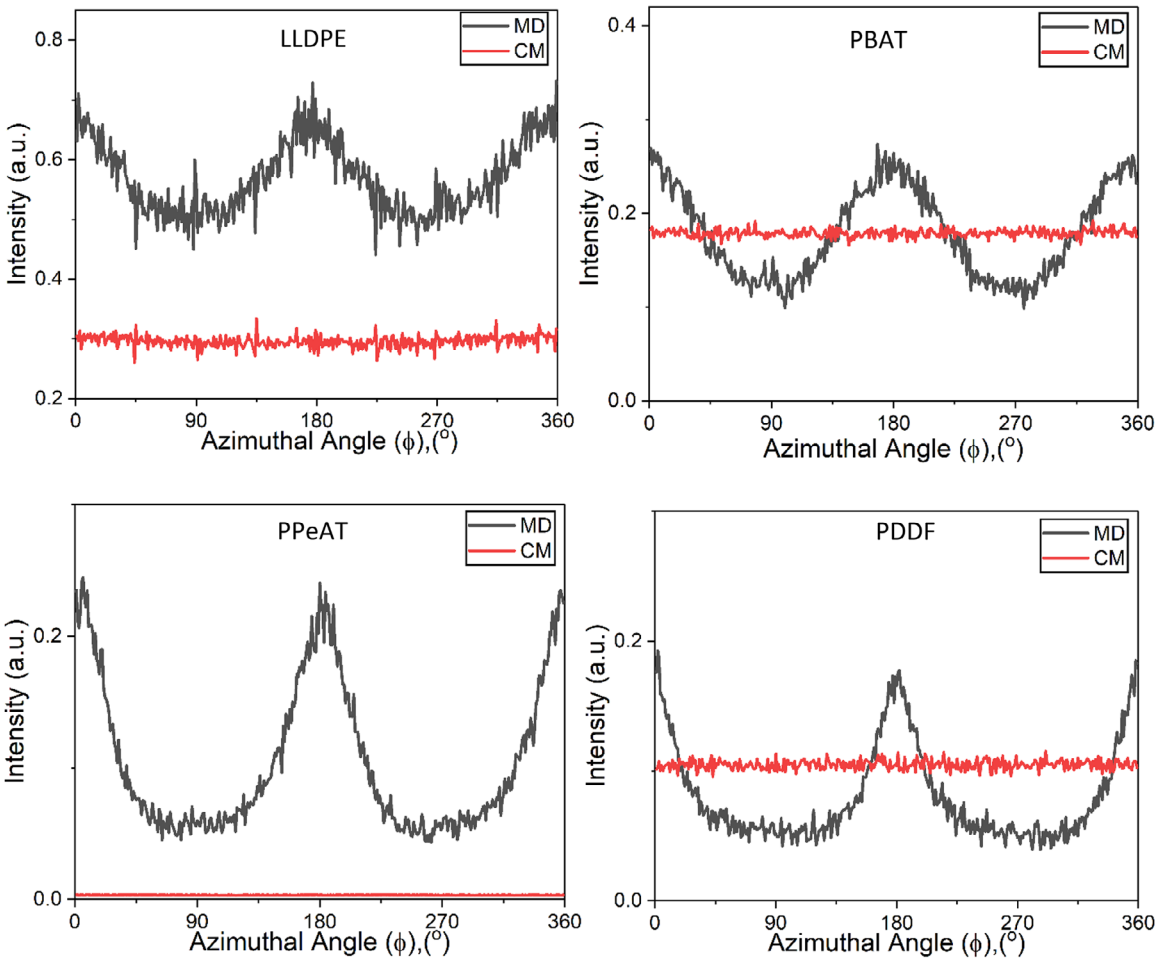

FIGURE 5 | Film orientation from small x-ray scattering for LLDPE, PBAT, PPeAT, and PDDF CMSs and BFs. An angle of 0° for the BFs corresponds to the MD.

results show that the lamellar thickness were also higher. PPeAT film had a smaller d-spacing and thinner lamellar thickness compared to PBAT film, consistent with results obtained from the CMSs. Additionally, PDDF CMS had a larger lamellar thickness compared with PBAT and PPeAT CMSs due to higher percent crystallinity of the former.

To observe the change in orientation between CMSs and BFs of LLDPE, PBAT, PPeAT, and PDDF, SAXS patterns in Figure 4 were examined for change in the transmissional intensities as a function of the azimuthal angle, with results shown in Figure 5. Scattering vector range used for orientation was 0.015–0.1 A^{-1} for LLDPE, 0.02–0.15 A^{-1} for PBAT, 0.03–0.1 A^{-1} for PPeAT, and 0.028–0.1 A^{-1} for PDDF and were chosen on the basis of only incorporating scattering that was part of the broad peak shown in Figure 3. Scattering intensities for BFs show a sinusoidal shape due to orientation of the lamellae normals, while for CMSs, the intensity is almost constant with respect to the azimuthal angle (∅). This observation is consistent with results in the literature [42]. The orientation parameter was calculated using (Equation 2) and reported in Table 2 [43]. More orientation can be observed for PPeAT BF compared with the roughly equivalent PDDF BF and PBAT BF. Much lower lamellar orientation was observed for LLDPE BF.

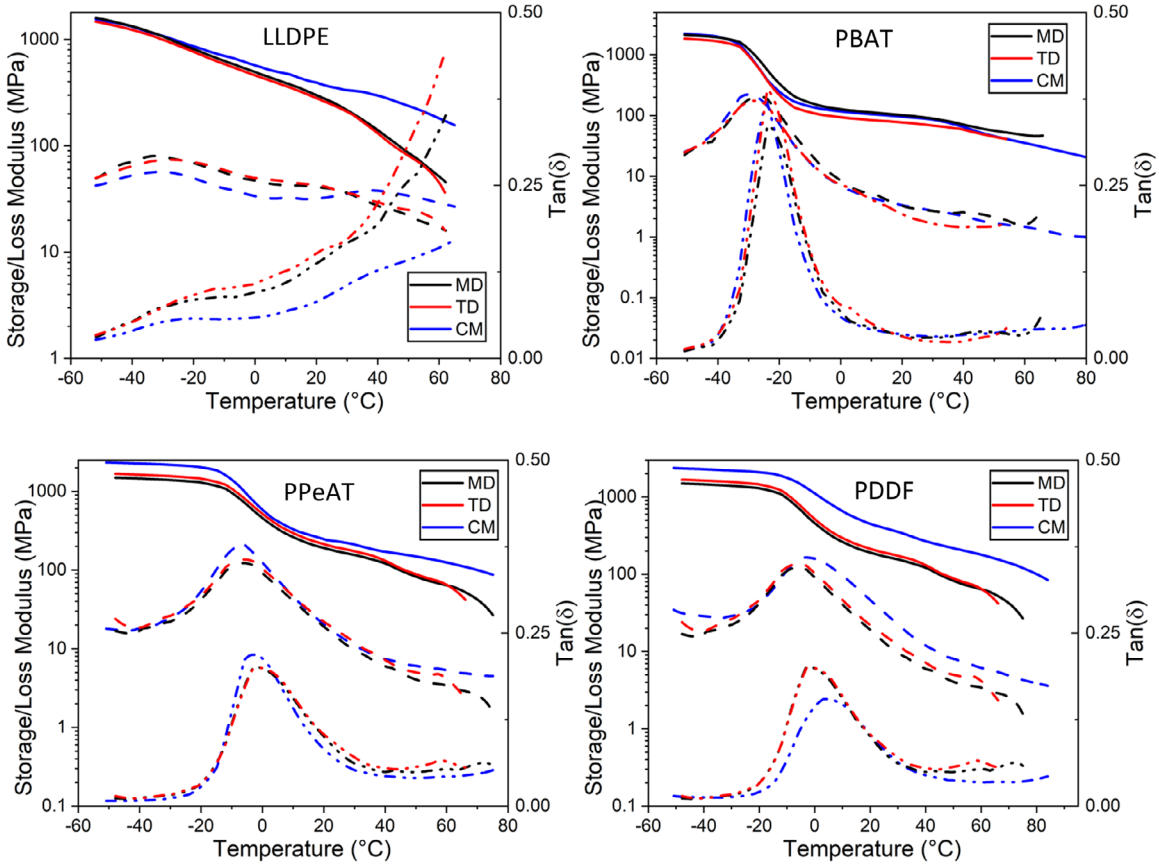

FIGURE 6 | Viscoelastic profile form Dynamic Mechanical Analyzer for LLDPE, PBAT, PPeAT, and PDDF CMSs and BFs. Storage modulus is represented as (- solid lines), loss modulus is represented as (- -dashed lines) and damping factor is represented as (-·-·dashed lines).

As orientation becomes more aligned with the MD, the values of $<\cos^2\varnothing>$ and the orientation factor approach 1, whereas alignment with the TD causes $<\cos^2\varnothing>$ to approach 0 and the orientation factor to approach −1/2. For random orientation, $<\cos^2\varnothing>$ is 1/3, and the orientation factor is 0 [43]. $<\cos^2\varnothing>$ and orientation factors for CMSs in all four polymers are approximately 0.33 and 0, respectively, confirming their random orientation.

For BF samples, normals for the crystalline lamellae are oriented more in the MD than in the TD. Higher orientation in the MD is consistent with the work of Bafna et al. [44], who investigated high-density polyethylene melt-blown film using an industrial scale film blower. The orientation factor in the machine direction increased from 0.352 for the smallest draw ratio to 0.585 for the highest draw ratio; our orientation factors are closer to the smaller draw ratio.

Although some degree crystal orientation in the MD was observed in PPeAT and PDDF, the orientation was not enough to cause differences in Young's moduli. However, lab-scale film blowers typically operate at lower drawdown ratios and slower cooling rates compared to industrial-scale film blowers, resulting in less pronounced molecular orientation. Stress at break and elongation at break results were not consistent with the different polymers in the MD and TD, indicating that if orientation effects were relevant, then this result must be a function of amorphous chain orientation, which was not measured here.

2.4 | Dynamic Mechanical Analysis (DMA)

Storage modulus (E'), loss modulus (E'') and damping factor (tan δ) as a function of temperature for CMSs as well as films cut with the long axis in the MD and TD are shown in Figure 6. For all four polymers, E' and E'' for the CMSs had a higher value than the BFs. No statistically significant differences existed for the films cut in the TD vs. MD. These results are consistent with the Young's modulus and degree of crystallinity results. The peak maximum of tan δ for the CMSs polyesters shifted to a lower temperature with respect to the BFs (MD and TD), which is an indication of a lower T_g. As previously mentioned, CMSs had a larger d-spacing than BFs. The decrease in d-spacing and lamellar thickness in BF was accompanied by a corresponding decrease in T_g [45, 46].

2.5 | Barrier Properties

Oxygen (P_{O_2}) and carbon dioxide (P_{CO_2}) permeabilities are shown in Table 3. P_{O_2} and P_{CO_2} for LLDPE and PBAT agree with the literature [47–49]. CMSs showed lower P_{O_2} and P_{CO_2} than BFs.

TABLE 3 | Oxygen and carbon dioxide permeation and WVTR results for LLDPE, PBAT, and PPeAT CMSs and BFs.

Samples		P_{O_2} Barrer	P_{CO_2} Barrer	WVTR g mm $m^{-2}d^{-1}$
LLDPE	CMS	2.65 ± 0.23	12.00 ± 1.06	0.099 ± 0.01
	BF	3.56 ± 0.32	14.50 ± 1.28	0.17 ± 0.10
PBAT	CMS	1.20 ± 0.20	12.55 ± 1.99	6.95 ± 0.21
	BF	1.30 ± 0.26	14.80 ± 2.98	10.86 ± 0.26
PPeAT	CMS	0.25 ±1 0.02	2.25 ± 0.21	1.44 ± 0.12
	BF	0.60 ± 0.11	4.31 ± 0.79	2.14 ± 0.34
PDDF	CMS	0.38 ± 0.03	2.13 ± 0.15	0.47 ± 0.06
	BF	0.58 ± 0.19	3.80 ± 1.30	1.08 ± 0.20

Kim et al. reported that BFs exhibit an increased permeability due to the more perpendicular orientation of spherulite lamellae arms to the film surface, whereas slowly cooled CMSs develop a higher percentage of parallel-oriented lamellae, resulting in lower permeability [50]. Also, Khanna et al. observed that the stretching of oriented films introduces mechanical defects and stresses, which also increases permeability [51]. Polyesters tend to have a lower P_{O_2} than polyolefins due to the presence of carbonyl and ester bonds, which lead to a more hydrophilic structure and thus a lower P_{O_2} [52]. As expected, PPeAT and PBAT had a lower P_{O_2} than LLDPE, making them good candidates for food packaging to maintain freshness and prevent staling. The decrease in gas permeability and water vapor transmission rate of CMS PPeAT compared to CMS PBAT can be attributed to several factors. The first factor is lamellar thickness. While PBAT exhibited a slightly higher percent crystallinity than that of PPeAT, the lamellar thickness of PPeAT was smaller. This reduced lamellar thickness translates to more numerous, smaller crystals, which resulted in a more tortuous pathway for diffusion. The second factor could be Đ; Đ of PPeAT is double Đ of PBAT which in turn will affect the orientation of the amorphous phase, which could be a factor in barrier properties improvement [53, 54]. The improved barrier properties of PDDF CMS compared with LLDPE CMS were due to the presence of carbonyl and ester bonds, which led to a more hydrophilic structure and thus a lower P_{O_2}. Liu et al. observed that the increase in oxygen/carbon ratio in the repeating unit of a polymer structure will lead to an increase in P_{CO_2} relative to other gases [55]. Since PPeAT has a higher oxygen/carbon ratio than PDDF, PPeAT CMS showed a lower P_{O_2} but a higher P_{CO_2} compared with PDDF CMS. Additionally, PDDF BF exhibits a lower P_{O_2} and lower P_{CO_2} compared with PPeAT BF due to the higher percent crystallinity of the PDDF BF.

Water vapor transmission rates (WVTR) for LLDPE, PBAT and PPeAT are also shown in Table 3. CMSs exhibited a lower WVTR compared to BFs, following the same trend as P_{O_2} and P_{CO_2}. PBAT, PPeAT and PDDF had a higher WVTR than LLDPE due to the hydrophilic nature of the polar functional groups, such as hydroxyl, ester and carboxyl groups, which form hydrogen bonds with water vapor molecules [56]. PPeAT exhibited a lower WVTR than PBAT again likely due to a more tortuous pathway due to smaller and more numerous crystals. Furthermore, PDDF had a significantly lower WVTR than PBAT and PPeAT, likely due to higher percent crystallinity since the diffusion constant of water through an amorphous polymer will be much larger than the diffusion rate through a crystalline polymer [57, 58].

3 | Conclusions

PPeAT and PDDF were successfully film blown using a lab scale film blower and were compared with film blown commercial LLDPE and commercial PBAT. Blown films (BFs) showed a reduced Young's modulus and storage modulus compared with compression molded sheets (CMSs), consistent with the measured higher crystallinites of the latter. No statistically significant difference was found with the Young's modulus for films cut with the long axis in the MD and TD, while a higher elongation at break was found in the TD, except for PDDF, where the opposite held true. CMSs exhibited longer d-spacings, larger lamellar thicknesses and lower glass transition temperatures compared with BFs. CMSs had lower oxygen permeabilities, carbon dioxide permeabilities and water vapor transmission rates compared with BFs. PPeAT showed lower oxygen and carbon dioxide permeabilities compared with PBAT and LLDPE and lower water vapor transmission rate than PBAT, which is attributed to orientation coupled with the effect of lamellar thickness and molecular weight dispersity. PPeAT showed a lower oxygen permeability, and a higher carbon dioxide permeability compared to PDDF, consistent with the higher oxygen/carbon ratio. Film blown PPeAT and PDDF showed promising results and could potentially be used as a drop-in replacement for LLDE/LDPE in flexible film packaging.

4 | Experimental Section

4.1 | Materials

A sodium-neutralized ethylene-methacrylic acid ionomer was used as nucleating agent and was graciously provided by DuPont (now Dow). For PDDF, 1,12 dodecanediol (DD, thermos scientific) 2,5-furandicarboxylic acid (FA, Accela), and also titanium (IV) isopropoxide (Acros Organics) were used. Film grade LLDPE with an MFI of 2 g 10 min^{-1} (ExxonMobil LL1002.YB) and PBAT (BASF Ecofle C1200) were also tested. LLDPE was kindly provided by Amcor plc and PBAT was purchased from Azelis Americas. Based on the measured glass and melting temperatures measured in our lab [21], and data published here [59], m and n for PBAT were both 0.5. All chemicals were used as received.

High molecular weight PPeAT was synthesized in our lab via direct esterification and polycondensation, following a method previously developed and published by our group [60]. Number average molecular weight, weight average molecular and dispersity (Đ) for PPeAT were 69,900 g mol^{-1}, 219,000 g mol^{-1} and 3.13, respectively. A similar procedure was used for PDDF, number average molecular weight, weight average molecular weight and Đ were 39,400 g mol^{-1}, 90,400 g mol^{-1} and 2.29, respectively.[23] These molecular weights were chosen because of their approximate equivalence in extensional viscosity at 130°C for the PBAT and LLDPE detailed elsewhere.[21, 23] 130°C has been shown to be a good analog for film blowing [61], Chemical structures of PBAT, PPeAT and PDDF are shown in Figure 7.

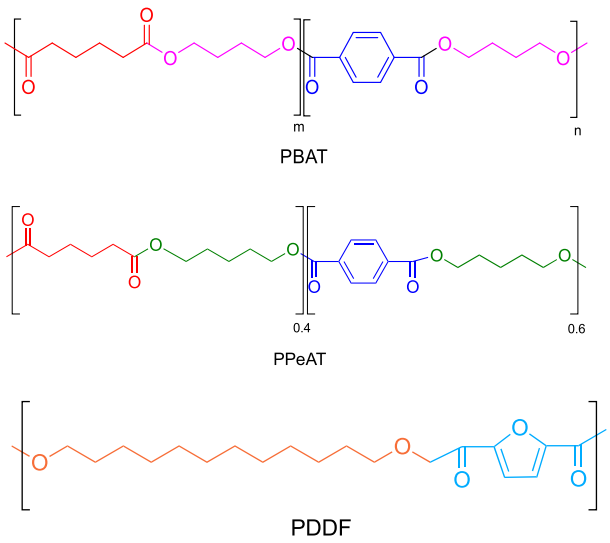

FIGURE 7 | Chemical structures of PBAT, PPeAT, and PDDF.

4.2 | Nucleator Addition

PPeAT and an ionomer nucleator were dried in a vacuum oven at room temperature for 24 h prior to film formation to remove residual moisture. The ionomer nucleator used was ethylene with methacrylic acid partially neutralized with Na with 78.4% neutralization and melt index of 1.26. To add nucleator, PPeAT was melt-mixed with 0.5% w/w ionomer using a 1″ Killion single screw extruder with 24/1 L/D ratio. The 3-barrel heating zones were set to 135/135/135°C and the die heating zone was 120°C while the screw speed was 60 RPM. The extruded strand was cooled using a water/ice bath and fed to a pelletizer to pelletize the nucleated PPeAT as shown in Figure 8. These conditions yielded good dispersion of the nucleator within the PPeAT as evidenced by the equivalence of crystallization kinetics using this mixing technique compared to mixing with a conical twin screw (results not shown). Also, FTIR spectra shown in the Supplemental Information show no changes in FTIR spectra other than those related to differences in crystallinity; the nucleator is in such low concentration that FTIR is not sensitive enough to see such interactions (e.g. changes in hydrogen bonding for example).

No nucleator was added to PDDF due to its inherently fast crystallization rate. Nevertheless, the polymer was extruded under identical conditions to produce pellets for the subsequent film-blowing process. Since PBAT and LLDPE were already in the form of pellets, no extrusion in our laboratories was necessary.

4.3 | Film Preparation

Pellets were fed to a LE8-30/C conical single screw extruder (30/1 L/D ratio) fitted with a LUMF-150 ultra microfilm blowing tower from Labtech engineering. The heating barrel temperature was set to 210°C while the die heating temperature was set to 200°C. Lower processing temperatures led to excessive melt viscosity which overloaded the extruder's motor. The annular die was 20 mm in diameter and the blow-up ratio (BUR) was set to 3.5. The other parameters were adjusted to produce an average bubble thickness between 0.05 and 0.06 mm for all samples. Hence, the screw speed, air blower, haul-off speed and pull roll and winder speed were set to 300 RPM, 1020 RPM, 4.9 ft min^{-1} and 29.4 ft min^{-1}, respectively for LLDPE and 100 RPM, 2000 RPM, 2 ft min^{-1} and 15 ft min^{-1}, respectively for the PPeAT, PBAT, and PDDF. The air blower used room temperature air, and no external forced convection air cooling was used. Pictures of film bubbles for all resins are shown in Figure 9. CMSs with thicknesses between 0.4 and 0.5 mm were produced via a Carver laboratory press operated at 5 metric tons and a temperature of 180°C.

4.4 | Polymer Characterization

A 200 lb. SSTM tester from United Testing Systems was used to measure mechanical properties at room temperature. A dog-bone shaped sample according to the ASTM D-1708 standard was cut from CMSs and BFs with 1.27 cm min^{-1} rate of straining and dogbone gauge length of 2.2 cm. An average of 7 samples were used to calculate the final tensile properties of polymers.

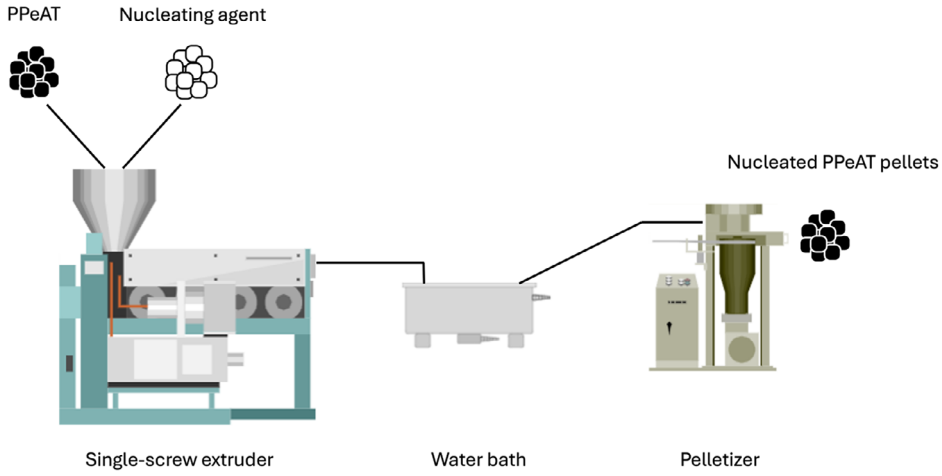

FIGURE 8 | Schematic representation of melt compounding process using a single screw extruder.

FIGURE 9 | Stable film bubble from LUMF-150 for LLDPE, PBAT, PPeAT, and PDDF.

Wide-angle x-ray scattering (WAXS) and small-angle x-ray scattering (SAXS) measurements were performed using a Xenocs XEUSS 3.0 with Cu-K-alpha radiation (1.54 Å). The apparatus was operated at 50 kV and 0.6 mA with a q-range of 0.15–3.4 $Å^{-1}$ and 0.01–0.3 $Å^{-1}$ with an exposure time of 60 and 120 min for WAXS and SAXS, respectively. 1D-WAXS and SAXS profiles were obtained from circularly integrated intensities of acquired 2D-WAXS and SAXS images, respectively. Patterns for MD and TD were calculated for ±5° around the appropriate axis. To calculate the fractional crystallinity from the circularly-averaged WAXS pattern for the overall crystallinity or from the MD and TD patterns, a program was used to fit a linear baseline followed by a Gaussian curve to each peak and the amorphous halo. For evaluation of the orientation factor (f) at a given scattering angle range, a quantitative measurement was carried out using the Herman's orientation function shown in (Equation 2).

$$f = \frac{3\left\langle \cos^2 \emptyset \right\rangle - 1}{2} \tag{2}$$

where,

$$\left\langle \cos^2 \emptyset \right\rangle = \frac{\int_0^{\frac{\pi}{2}} I(\emptyset) . \sin \emptyset . \cos^2 \emptyset d\emptyset}{\int_0^{\frac{\pi}{2}} I(\emptyset) . \sin \emptyset d\emptyset} \tag{3}$$

$\langle \cos^2 \varnothing \rangle$ is the average cosine square of the angles between the oriented molecular chain and the drawing direction and $I(\varnothing)$ is the baseline subtracted intensity distribution around the azimuthal angle.

Dynamic mechanical analysis (DMA) for the BFs (both MD and TD) and CMSs were performed using a linear tension fixture geometry on the TA instruments Ares G2. The test was conducted at a temperature range of -50°C to the sample melting temperature, a frequency of 1 Hz, strain of 0.02% and a temperature step of 3°C. In all cases, tests were done in the linear viscoelastic region.

CO_2 and O_2 permeabilities of the CMSs and BFs were measured at 1 bar and 25°C in a constant volume, variable pressure barometric device with a 47 mm HP filter holder. Prior to the experiment, the system was left under vacuum for 24 h to remove any humidity and previously absorbed gases. Upstream pressure was monitored using a PX-409-USHB pressure transducer with a full-scale of 1000 psi while the downstream pressure was monitored using another PX-409-USHB with a full scale of 260 torr. The change in downstream pressure over time was recorded and the permeability (P) at steady state can be calculated using (Equation 4):

$$\mathrm{P} = \frac{lV_{down}}{ART\Delta p} . \frac{dp}{dt}_{down} \tag{4}$$

where, l and A are the thickness and the area of the film, respectively, R is the universal gas constant, T is the absolute temperature, V_{down} is the downstream volume, Δp is the pressure difference across the film, and $\frac{dp}{dt}_{down}$ is the steady state slope of pressure versus time in the downstream.

Water vapor transmission rate (WVTR) was measured according to ASTM E96 (dry cup method) by first fixing a dry sample (of mass m_0) on a vial filled with desiccant ($CaSO_4$) in a desiccator saturated with water vapor and then monitoring the increase in mass (m_g) as a function of exposure time. The vials covered with the film were weighed at certain times until 21 days. Weight changes of the vial were plotted vs. times, and then the slopes of the plot of each sample were obtained. The thickness and area of each sample were measured prior to testing. WVTR was calculated using (Equation 5):

$$WVTR = \left.\frac{dm_g}{dt}\right|_{s.s} . \frac{l}{A} \tag{5}$$

where $\left.\frac{dm_g}{dt}\right|_{s.s}$ is the steady state slope of mass gained versus time, while l and A are the thickness and the area of the film, respectively.

Acknowledgements

This work was supported by the Department of Energy under Grant Agreement number DE-EE0009305. The authors also gratefully acknowledge the National Science Foundation (CMMI-2216074) and the Univer-

sity of Tulsa for funds contributing to the purchase of theSAXS/WAXS. Financial support for publication costs was provided by the University of Oklahoma Libraries' Open Access Fund. The authors would like to thank Lucas Condes and Mathew Webb for help with the permeability measurements.

Conflicts of Interest

GWH has a financial interest in Pyran which is commercializing the technology to produce biomass-based 1,5 pentanediol.

Data Availability Statement

The data that support the findings of this study are available from the corresponding author upon reasonable request.

References

1. V. Manzano, N. L. García, C. R. Ramírez, N. D'Accorso, and S. Goyanes, "Mulch Plastic Systems: Recent Advances and Applications," in *Polymers for Agri-Food Applications*, ed. T. J. Gutiérrez, (Springer International Publishing, 2019): 265–290.

2. D. A. K. Putri, Ismadi, D. Purnomo, et al., "Mechanical and Thermal Characteristics of Mulch Film Derived from Linear Low-Density Poly Ethylene (LLDPE) with the Addition of Lignin or Coconut Coir Powder," *AIP Conference Proceedings* 2973 (2024): 050001.

3. O. Delgadillo-Velázquez, S. G. Hatzikiriakos, and M. Sentmanat, "Thermorheological Properties of LLDPE/LDPE Blends: Effects of Production Technology of LLDPE," *Journal of Polymer Science Part B: Polymer Physics* 46, no. 16 (2008): 1669–1683.

4. S. Ronca, "Chapter 10-Polyethylene," in *Brydson's Plastics Materials*, (Eighth Edition), ed. M. Gilbert, (Butterworth-Heinemann, 2017): 247–278.

5. Z. Yao, H. J. Seong, and Y. S. Jang, "Environmental Toxicity and Decomposition of Polyethylene," *Ecotoxicology and Environmental Safety* 242 (2022): 113933.

6. G. A. O. Tiago, A. Mariquito, S. Martins-Dias, and A. C. Marques, "The Problem of Polyethylene Waste – Recent Attempts for Its Mitigation," *Science of The Total Environment* 892 (2023): 164629.

7. B. Zhang, X. Yang, L. Chen, J. Chao, J. Teng, and Q. Wang, "Microplastics in Soils: A Review of Possible Sources, Analytical Methods and Ecological Impacts," *Journal of Chemical Technology & Biotechnology* 95, no. 8 (2020): 2052–2068.

8. P. Wanner, "Plastic in Agricultural Soils – A Global Risk for Groundwater Systems and Drinking Water Supplies? – A Review," *Chemosphere* 264 (2021): 128453.

9. E. Liwarska-Bizukojc, "Effect of (bio)Plastics on Soil Environment: A Review," *Science of The Total Environment* 795 (2021): 148889.

10. J. M. Millican and S. Agarwal, "Plastic Pollution: As Material Problem?," *Macromolecules* 54, no. 10 (2021): 4455–4469.

11. A. Samir, F. H. Ashour, A. A. A. Hakim, and M. Bassyouni, "Recent Advances in Biodegradable Polymers for Sustainable Applications," *npj Materials Degradation* 6 (2022): 68.

12. Y. Yang, J. Min, T. Xue, et al., "Complete Bio-Degradation of Poly(butylene adipate-co-terephthalate) via Engineered Cutinases," *Nature Communications* 14, no. 1 (2023): 1645.

13. J. Jian, Z. Xiangbin, and H. Xianbo, "An Overview on Synthesis, Properties and Applications of Poly(butylene-adipate-co-terephthalate)–PBAT," *Advanced Industrial and Engineering Polymer Research* 3 (2020): 19–26.

14. R. Qi, D. L. Jones, Q. Liu, Q. Liu, Z. Li, and C. Yan, "Field Test on the Biodegradation of Poly(butylene adipate-co-terephthalate) Based Mulch Films in Soil," *Polymer Testing* 93 (2021): 107009.

15. A. Teamsinsungvon, Y. Ruksakulpiwat, and K. Jarukumjorn, "Preparation and Characterization of Poly(lactic acid)/Poly(butylene adipate-co-terepthalate) Blends and Their Composite," *Polymer-Plastics Technology and Engineering* 52 (2013): 1362–1367.

16. J. Andrzejewski, J. Cheng, A. Anstey, A. K. Mohanty, and M. Misra, "Development of Toughened Blends of Poly(lactic acid) and Poly(butylene adipate-co-terephthalate) for 3D Printing Applications: Compatibilization Methods and Material Performance Evaluation," *ACS Sustainable Chemistry & Engineering* 8, no. 17 (2020): 6576–6589.

17. *Ecoflex (PBAT)*, https://plastics-rubber.basf.com/global/en/performance_polymers/products/ecoflex (Accessed August 2024).

18. *Mater-Bi (PBAT)*, https://www.novamont.com/eng/mater-bi (Accessed August 2024).

19. *COMPOSTFUL*, https://www.lgchem.com/product-detail/compostful (Accessed August 2024).

20. *High-strength PBAT*, https://www.skc.kr/eng/creation/detailView.do?menuCd=002007&lang=eng&cate1=291&cate2=363&cate3=&cate4= (Accessed August 2024).

21. H. Aboukeila, O. Singh, J. Klier, G. W. Huber, and B. P. Grady, "Synthesis and Characterization of Biobased Copolyesters Based on Pentanediol: (2) Poly(pentylene adipate-co-terephthalate)," *Polymer Engineering & Science* 64, no. 10 (2024): 4746–4759.

22. L. Zheng, M. S. Kim, S. Xu, M. Urgun-Demirtas, G. W. Huber, and J. Klier, "Biodegradable High-Molecular-Weight Poly(pentylene adipate-co-terephthalate): Synthesis, Thermo-Mechanical Properties, Microstructures, and Biodegradation," *ACS Sustainable Chemistry & Engineering* 11, no. 38 (2023): 13885–13895.

23. H. Aboukeila, E. R. Chokkapu, H.-F. Tu, et al., "Biobased Poly(dodecylene furanoate) with Inherent Advantages in Performance and Circularity," *Chemsuschem* 18 (2025): 202501080.

24. B. A. Morris, "2—Converting Processes," in *The Science and Technology of Flexible Packaging*, (William Andrew Publishing, 2017), 10.1016/B978-0-323-24273-8.00002-2.

25. D. V. Rosato, "Extruding Plastics," in *A Practical Processing Handbook*, (Springer Publishing, 2017).

26. J. Vlachopoulos, R. Castillo, N. D. Polychronopoulos, and S. Tanifuji, "Blown Film Dies," in *Design of Extrusion Forming Tools*, (Smithers Rapra, 2012).

27. B. Le Delliou, O. Vitrac, A. Benihya, A. Guinault, and S. Domenek, "Development of Extrusion Blown Films of Poly(3-hydroxybutyrate-co-3-hydroxyvalerate) Blends for Flexible Packaging," *Journal of Applied Polymer Science* 141, no. 16 (2024): 55240.

28. M. C. Mistretta, L. Botta, F. P. La Mantia, A. Di Fiore, and M. Cascone, "Film Blowing of Biodegradable Polymer Nanocomposites for Agricultural Applications," *Macromolecular Materials and Engineering* 306, no. 9 (2021): 2100177.

29. R. K. Krishnaswamy and A. M. Sukhadia, "Orientation Characteristics of LLDPE Blown Films and Their Implications on Elmendorf Tear Performance," *Polymer* 41, no. 26 (2000): 9205–9217.

30. A. Bashirgonbadi, L. Delva, E. Caron, F. H. Marchesini, K. M. Van Geem, and K. Ragaert, "The Interplay Between Macromolecular Structure, Rheology, Processing Condition, and Morphology for (linear) Low Density Polyethylenes in Film Blowing," *Polymer* 290 (2024): 126566.

31. G. Gururajan and A. A. Ogale, "Real-time Crystalline Orientation Measurements during Low-density Polyethylene Blown Film Extrusion Using Wide-angle X-ray Diffraction," *Polymer Engineering & Science* 52, no. 7 (2012): 1532–1536.

32. C. Ge, C. Fortuna, K. Lei, and L.-X. Lu, "Neat EVOH and EVOH/LDPE Blend Centered Three-layer co-extruded Blown Film without Tie Layers," *Food Packaging and Shelf Life* 8 (2016): 33–40.

33. C. C. Chau and W. R. LaFollette, "Shear Yielding in Blown Oriented Polystyrene Films," *Advanced Materials* 12, no. 23 (2000): 1859–1864.

34. M. Harth and A. Dornhofer, "Film Blowing of Linear and Long-Chain Branched Poly(ethylene terephthalate)," *Polymers (Basel)* 12, no. 7 (2020): 1605.

35. B. E. Itabana, A. K. Pal, A. K. Mohanty, and M. Misra, "Biodegradable Blown Film Composite from Poly (Butylene Adipate-co-Terephthalate) and Talc: Effect of Uniaxial Stretching on Mechanical and Barrier Properties," *Food Packaging and Shelf Life* 39 (2023): 101147.

36. Y. Jiang, C. Yan, K. Wang, D. Shi, Z. Liu, and M. Yang, "Super-Toughed PLA Blown Film with Enhanced Gas Barrier Property Available for Packaging and Agricultural Applications," *Materials* 12, no. 10 (2019): 1663.

37. P. F. Teixeira, J. A. Covas, M. J. Suarez, et al., "Film Blowing of PHB-Based Systems for Home Compostable Food Packaging," *International Polymer Processing* 35 (2020): 101147.

38. M. Rajabi, A. Ali, M. McConnell, and J. Cabral, "Keratinous Materials: Structures and Functions in Biomedical Applications," *Materials Science and Engineering: C* 110 (2020): 110612.

39. S. Auksornkul, S. Soontaranon, C. Kaewhan, et al., "Effect of the Blow-up Ratio on Morphology and Engineering Properties of Three-layered Linear Low-density Polyethylene Blown Films," *Journal of Plastic Film & Sheeting* 34, no. 1 (2017): 27–42.

40. E. Mejia, N. Cherupurakal, A. I. Mourad, S. Al Hassanieh, and M. Rabia, "Effect of Processing Techniques on the Microstructure and Mechanical Performance of High-Density Polyethylene," *Polymers (Basel)* 13, no. 19 (2021): 3346.

41. C. Hedesiu, D. E. Demco, R. Kleppinger, et al., "The Effect of Temperature and Annealing on the Phase Composition, Molecular Mobility and the Thickness of Domains in High-density Polyethylene," *Polymer* 48, no. 3 (2007): 763–777.

42. Y. Ren, Y. Shi, X. Yao, Y. Tang, and L. Z. Liu, "Different Dependence of Tear Strength on Film Orientation of LLDPE Made with Different Co-Monomer," *Polymers* 11, no. 3 (2019): 434.

43. L. E. Alexander, "X-ray Diffraction Methods in Polymer Science," in *Journal of Materials Science*, (Wiley-Interscience, 1969).

44. A. Bafna, D. McFaddin, G. Beaucage, J. Merrick-Mack, and F. M. Mirabella, "Integrated Mechanism for the Morphological Structure Development in HDPE Melt-Blown and Machine-Direction-Oriented Films," *Journal of Polymer Science Part B: Polymer Physics* 45, no. 14 (2007): 1834–1844.

45. Z. Bashir and S. Rastogi, "The Explanation of the Increase in Slope at the Tg in the Plot of D-Spacing Versus Temperature in Polyacrylonitrile," *Journal of Macromolecular Science, Part B* 44 (1) (2014): 55–78.

46. P. Wojciechowski, "Thermotropic Mesomorphism of (2-Hydroxypropyl)Cellulose Systems-the Role of Hydrophilic and Lipophilic Segments," *Molecular Crystals and Liquid Crystals Science and Technology. Section A. Molecular Crystals and Liquid Crystals* 354, no. 1 (2000): 309–317.

47. P. Qin, L. Wu, B. Li, N. Li, X. Pan, and J. Dai, "Superior Gas Barrier Properties of Biodegradable PBST vs," *PBAT Copolyesters: A Comparative Study* 13, no. 19 (2021): 3449.

48. Y. Wang, A. J. Easteal, and X. D. Chen, "Ethylene and Oxygen Permeability through Polyethylene Packaging Films," *Packaging Technology and Science* 11, no. 4 (1998): 169–178.

49. M. R. Kamal, I. A. Jinnah, and L. A. Utracki, "Permeability of Oxygen and Water Vapor through Polyethylene/Polyamide Films," *Polymer Engineering & Science* 24, no. 17 (1984): 1337–1347.

50. K. Kim, A. J. Zervoudakis, J. A. LaNasa, et al., "Polyethylene Blends for Improved Oxygen Barrier: Processing-Dependent Microstructure and Gas Permeability," *ACS Applied Polymer Materials* 6 (2023): 524–533.

51. Y. P. Khanna, E. D. Day, M. L. Tsai, et al., "Re-Examining the Oxygen Barrier of Nylon 6 Films. I. Role of Moisture and Processing Induced Variables," *Journal of Plastic Film & Sheeting* 13, no. 3 (1997): 197–211.

52. N. Bumbudsanpharoke, P. Wongphan, K. Promhuad, P. Leelaphiwat, and N. Harnkarnsujarit, "Morphology and Permeability of Bio-Based Poly(butylene adipate-co-terephthalate) (PBAT), Poly(butylene succinate) (PBS) and Linear Low-Density Polyethylene (LLDPE) Blend Films Control Shelf-Life of Packaged Bread," *Food Control* 132 (2022): 108541.

53. S. Wang, S. Jin, X. Han, et al., "Insights into the Relationship Between Structure and Properties of Spirobichroman-Based Polyimides: Effects of Substituents on Molecular Structure and Gas Separation," *Materials & Design* 194 (2020): 108933.

54. G. Stoclet, S. Xu, V. Gaucher, et al., "Influence of the Molecular Weight on Mechanical Behavior and Associated Strain-induced Structural Evolution of Poly(ethylene 2,5-furandicarboxylate) Upon Biaxial Stretching," *Polymer* 217 (2021): 123441.

55. J. Liu, G. Zhang, K. Clark, and H. Lin, "Maximizing Ether Oxygen Content in Polymers for Membrane CO 2 Removal from Natural Gas," *ACS Applied Materials & Interfaces* 11, no. 11 (2019): 10933–10940.

56. S. Hemsri, K. P. Puttiwanit, K. Saeaung, and P. Satung, "Low Density Polyethylene/Poly(butylene adipate-co-terephthalate) Films: Effect of a Compatibilizer on Morphology and Properties," *International Conference on Engineering and Industrial Technology* 965 (2020): 012020.

57. J. Trifol, D. Plackett, P. Szabo, A. E. Daugaard, and M. Giacinti Baschetti, "Effect of Crystallinity on Water Vapor Sorption, Diffusion, and Permeation of PLA-Based Nanocomposites," *ACS Omega* 5, no. 25 (2020): 15362–15369.

58. Z. Dai, H. Aboukeila, L. Ansaloni, J. Deng, M. Giacinti Baschetti, and L. Deng, "Nafion/PEG Hybrid Membrane for CO2 Separation: Effect of PEG on Membrane Micro-structure and Performance," *Separation and Purification Technology* 214 (2019): 67–77.

59. R. Herrera, L. Franco, A. Rodríguez-Galán, and J. Puiggalí, "Characterization and Degradation Behavior of Poly(butylene adipate- co -terephthalate)s," *Journal of Polymer Science Part A: Polymer Chemistry* 40, no. 23 (2002): 4141–4157.

60. O. Singh, H. Aboukeila, J. Klier, G. W. Huber, and B. P. Grady, "Synthesis and Characterization of Biobased Copolyesters Based on Pentane Diol. (1) Poly(pentylene dodecanoate-co-furandicarboxylate)," *Polymer Engineering & Science* 64 (2024): 4935–4946.

61. J. S. Schulze, T. P. Lodge, C. W. Macosko, et al., "A Comparison of Extensional Viscosity Measurements from Various RME Rheometers," *Rheologica Acta* 40, no. 5 (2001): 457–466.

Supporting Information

Additional supporting information can be found online in the Supporting Information section.

Supporting File: mame70099-sup-0001-SuppMat.docx.